ACS APPLIED MATERIALS & INTERFACES

Research Article

www.acsami.org

Improved Efficiency of a Large-Area Cu(In,Ga)Se_2 Solar Cell by a Nontoxic Hydrogen-Assisted Solid Se Vapor Selenization Process

Tsung-Ta Wu,[†,‡] Fan Hu,[†,‡] Jyun-Hong Huang,[‡,§] Chia-ho Chang,[‡] Chih-chung Lai,[†] Yu-Ting Yen,[†] Hou-Ying Huang,[∥] Hwen-Fen Hong,[∥] Zhiming M. Wang,[⊥] Chang-Hong Shen,*[,‡] Jia-Min Shieh,*[,‡] and Yu-Lun Chueh*[,†]

[†]Department of Materials Science and Engineering, National Tsing-Hua University, Hsinchu 30013, Taiwan

[‡]National Nano Device Laboratories, No. 26, Prosperity Road 1, Hsinchu 30078, Taiwan

[§]College of Photonic and Institute of Imaging and Biomedical Photonics, National Chiao Tung University, Tainan City 71150, Taiwan

[∥]Institute of Nuclear Energy Research Atomic Energy Council, No. 1000, Wenhua Road, Jiaan Village, Longtan Township, Taoyuan County 32546, Taiwan

[⊥]State Key Laboratory of Electronic Thin Films and Integrated Devices, University of Electronic Science and Technology of China, Chengdu, Sichuan 610054, P. R. China

Supporting Information

ABSTRACT: A nontoxic hydrogen-assisted solid Se vapor selenization process (HASVS) technique to achieve a large-area (40 × 30 cm^2) Cu(In,Ga)Se_2 (CIGS) solar panel with enhanced efficiencies from 7.1 to 10.8% (12.0% for active area) was demonstrated. The remarkable improvement of efficiency and fill factor comes from improved open circuit voltage (V_{oc}) and reduced dark current due to (1) decreased interface recombination raised from the formation of a widened buried homojunction with n-type Cd_{Cu} participation and (2) enhanced separation of electron and hole carriers resulting from the accumulation of Na atoms on the surface of the CIGS film. The effects of microstructural, compositional, and electrical characteristics with hydrogen-assisted Se vapor selenization, including interdiffusion of atoms and formation of buried homojunction, were examined in detail. This methodology can be also applied to CIS ($CuInSe_2$) thin film solar cells with enhanced efficiencies from 5.3% to 8.5% (9.4% for active area) and provides a facile approach to improve quality of CIGS and stimulate the nontoxic progress in the large scale CIGS PV industry.

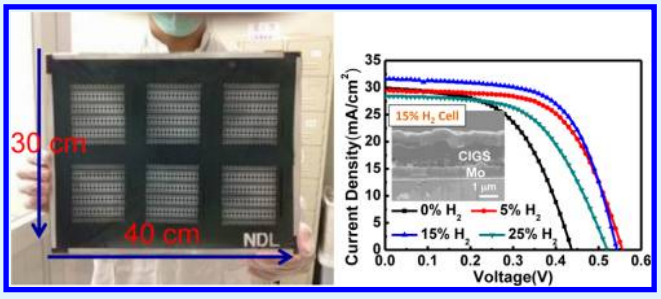

KEYWORDS: *Cu(In,Ga)Se_2, hydrogen-assisted selenization, buried homojunction, Na diffusion*

1. INTRODUCTION

Cu(In,Ga)$_2$Se (CIGS), the second generation thin film solar cell, has attracted much attention due to its lower cost, shorter energy payback time, better stability, and higher absorption coefficient with direct band gap feature, leading to CIGS solar cells with excellent performance and high commercial potential manufacturing, compared with silicon-based devices.[1,2] The highest efficiency of ~20.4% for the CIGS single cell fabricated by the three stage coevaporation process has already been demonstrated.[3] Advantages from this process, including controllably stoichiometric compositions, smoother surface, higher light absorption, and better carriers collection because of double-graded band gap engineering, result in a high quality CIGS absorber. However, poor uniformity in large scale limits this methodology for mass production.

The sputtering process *via* Cu/In/Ga metallic precursors followed by a selenization process is an alternative fabrication process of the CIGS thin film solar cell. Basically, two kinds of sources, namely solid selenium (Se) vapor and H_2Se gas, were used for the selenization process. The H_2Se gas is usually considered as the best candidate to achieve better concentration distribution, leading to enhanced efficiency due to the higher reaction activity of the Se-contained gas in the H_2Se ambient with the best conversion efficiency over 15%. However, safety concerns owing to toxic issues and facility cost have to be taken into account.[4,5] A carrier gas to carry Se vapors from heated Se pellets onto the substrate is relatively a nontoxic methodology, while a poor reactivity due to an inertly chemical feature of the Se element leads to formation of a nonstoichiometric Se concentration gradient in depth during the selenization process, resulting in a much higher defect density, thus the lower conversion efficiency of <11%.[6,7]

Received: December 17, 2013
Accepted: February 26, 2014
Published: February 26, 2014

Hydrogen (H_2) treatment in a solar cell has already been explored by many groups. For example, reduction of defect density for an amorphous-Si thin film solar cell can be achieved after the H_2 treatment due to passivation of Si dangling bonds by hydrogen atoms.[8] The function of the H_2 gas was also applied in the CI(G)S thin film solar cells, including reduction of deep level defects and removal of the oxidized surface on the CIGS thin film to improve the quality of p-n junction.[9−11] In addition, a hydrogen-containing solution as a reduction agent to enhance the quality of the CIGS thin film has been applied for the nonvacuum CIGS process.[12]

In this regard, we demonstrate a nontoxic hydrogen-assisted solid Se vapor selenization process (HASVS) technique using nontoxic Se pellets as a precursor to achieve a large-area (40 × 30 cm^2) and uniform CIGS solar panel with enhanced efficiencies from 7.1 to 10.8% where the term, "nontoxic", was confirmed by sensing the exhausting gas with H_2Se concentration of <1 ppb, which is detected by a commercial detector regularly. The HASVS process with a controllable N_2/H_2 ratio can promote the diffusion of solid Se atoms into the substrate, resulting in the formation of the CIGS film with low defect density confirmed by photoluminescence (PL) mapping, time-resolved photoluminescence (TRPL), and depth drive level capacitance profiling (DLCP) measurements. The smoother surface after the HASVS process was observed by scanning electron microscopy (SEM). An obvious diffusion of sodium atoms from the substrate to the CIGS film resulting in a widened Cu-poor region accompanied with diffusion of Cd atoms from the CdS layer, namely an inversion layer on the top surface of the CIGS thin film, was observed by X-ray photoelectron spectrometer (XPS) and secondary ion mass spectrometry (SIMS). The formation of the inversion layer was observed by transmission electron microscopy (TEM) and XPS spectra. The single step HASVS process without additional hydrogen treatment can fulfill the demand of uniformity in larger scale with lower cost.

2. EXPERIMENTAL SECTION

2.1. CIGS Solar Cell Fabrication. Configuration of a CIGS solar cell typically consists of SLG/Mo/CIGS/CdS/ZnO/ITO/Al. To achieve a stable and high efficiency CIS thin film solar cell, it is necessary to control related layers to standardize baseline specification. A soda lime Glass (SLG) with a moderate concentration of Na ions was used as substrate. A Mo back electrode on the SLG with a thickness of 0.4 μm was fabricated by two-stage sputtering processes to achieve better adhesion, higher thermal stability, and lower contact resistance.[13] The growth of the CIGS absorber layer was prepared by DC sputtering of CuGa and In metallic targets with a total thickness of ~0.8 μm, followed by the nontoxic hydrogen-assisted Se solid vapor selenization process (570 °C/20 min) with nontoxic Se pellets in a carrier gas of pure N_2 (denoted as 0% H_2) and ambient gas of N_2/H_2 with a varied ratio (denoted as 5% H_2, 15% H_2, and 25% H_2), respectively. The process pressure is about 80 Torr, and the concentration of Se is about 2.5% (Se vapor pressure is well-controlled by Se crucible temperature, which is about 2 Torr at 350 °C). A CdS buffer layer (transmittance >80%) with a thickness of ~80 nm was chemically grown on the CIGS layer *via* chemical bath deposition (CBD) at 70 °C with the growth time of 40 min. Subsequently, ZnO (70 nm)/ITO (550 nm) layers were deposited by pulsed-DC and DC sputtering systems as window/transparent conducting layers, respectively, with which the average transmittance >88% and resistivity <6.0 × 10^{-4} Ω-cm can be achieved. Finally, a top Al electrode with a thickness of 1 μm was deposited by the DC sputtering system.

2.2. Characterization. Morphology, microstructures, and atomic compositions of CIGS thin films were performed by field emission scanning electron microscopy (FESEM JSE-6500F) and high resolution transmission electron microscopy (HRTEM JEOL-3000F 300 kV) equipped with electron dispersive spectrometer (EDS). X-ray photoelectron spectroscopy (XPS, Thermo Fisher Scientific Theta Probe) was used to detect the compositional changes and bonding characteristics in the surface of the CIGS film. The compositional changes in depth were inspected by secondary ion mass spectrometry (SIMS, IMS 7F, CAMECA). Drive level capacitance profiling (DLCP, iHR550) was measured to directly measure the density of state as the function of spatial position for assessment of free carrier density (carrier density). Time-resolved photoluminescence (TRPL, iHR550) was used to measure and identify electron−hole recombination and a lifetime of photoexcited carriers. Current−voltage characteristics were measured under a standard AM 1.5 illumination (Class AAA Solar Simulator, Newport) with a power of 1000W/m^2 using a Keithley 2400 source-meter. The temperature was actively controlled during the measurements and was 25 ± 1 °C. Photolumiscence (PL) mapping was used to inspect how the uniformity of our whole device with an excited laser wavelength and power of 808 nm and 30 W. PL mapping was recorded at an excited laser power of 0.3 W/cm^2 with an integral time of 120 s at 20 °C, for which the images are captured by Si-based CCD under a cooling system.

3. RESULTS AND DISCUSSION

3.1. Analyses of Microstructural and Compositional Changes after the Nontoxic Hydrogen-Assisted Solid Se Vapor Selenization Process. Figures 1(a) and 1(b) show top view SEM images of two CIGS samples after the HASVS process with 5% H_2 and in a pure N_2 ambient (0% H_2). The much rougher surface can be distinctly observed for the CIGS film after the selenization process in a pure N_2 ambient (0% H_2), while a significantly improved surface roughness can be achieved after the HASVS process (5% H_2). The corresponding optical images of CIGS panels (30 cm × 40 cm) are shown in insets of Figure 1(a) and Figure 1(b). An obviously contrasting difference with many dark spots on the CIGS sample after the selenization in a pure N_2 ambient can be found, which results

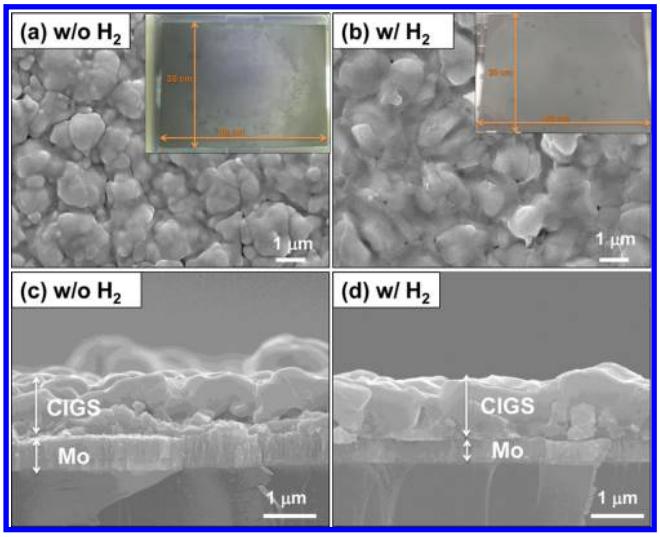

Figure 1. SEM images of (a) top view SEM images of CIGS film after the selenization process in the pure N_2 ambient. (b) Top view SEM of CIGS film after the hydrogen-assisted selenization process with 5% H_2 ambient. Insets in (a) and (b) show optical images of the CIGS film. (c) and (d) show the corresponding cross-sectional SEM images for CIGS films after the conventional selenization process in the pure N_2 ambient and the hydrogen-assisted selenization process in the 5% H_2 ambient.

from locally compositional deviation or unreacted regions because of an incomplete selenization process.[14] In contrast, the CIGS sample after the HASVS process (5% H_2) exhibits a significant enhancement with uniform contrast and less dark spots. The cross-sectional SEM images for both CIGS thin films are shown in Figure 1(c) and 1(d). Clearly, smoother surface and denser CIGS grains free of voids can be achieved for the sample after the HASVS process. Except for the different surface morphology and the grain size, the CIGS thin films after the HASVS process (5% H_2) and the pure N_2 ambient selenization process (0% H_2) exhibit almost the identical film thickness of ~1 μm with the same atomic composition ratios of bulk volume [Cu/(In+Ga)~0.8, Se~50%] inspected by SEM-EDS (Figure S1). In addition, preferred orientation at (112) without phase segregation and formation of other phases was confirmed from XRD spectra for both samples (Figure S2).

To shed light on how the HASVS process with different hydrogen partial pressures plays an important role on enhancement of film quality, the chemically bonding information for CIGS samples with the HASVS process and the conventional selenization in a pure N_2 ambient were acquired by XPS measurements as shown in Figures 2(a) to 2(c). We further characterize compositions of CIGS films after the HASVS process with different H_2/N_2 ratios and the selenization process in the pure N_2 ambient by XPS as shown in Table 1. Interestingly, a clear sodium (Na) peak located at 1071.3 eV with respect to Na 1s can be found, indicating that diffusion of Na from the SLG substrate by the HASVS process can be enhanced and the concentration of Na at the surface of the CIGS film increases with an increase of hydrogen concentrations (Figure 2a and Table 1) and the stronger oxygen intensity can be observed in the sample after the HASVS process as shown in Figure 2(b), for which O 1s is located at 531.2 eV. It is well-known that the original driving force of Na diffusion is most likely from the residual oxygen in the chamber since the Na facilitates the oxygenation process while more H_2 gas in the chamber might also reduce the amount of residual oxygen.[15] However, in our experiments, the function of H_2 may delay the oxidation process of the CISG during the selenization process, leading to more Na atoms diffusing out of the CIGS thin film surface.[16] However, the HASVS process causes formation of more In-oxide or Ga-oxide to shift from an oxygen bonding peak to lower binding energy. In addition, the indium (In) bonding peak from $CuInSe_2$ has a range from 444.6 eV (slightly Cu-poor of Cu:In:Se = 24.3:25.8:49.9) to 446.6 eV (severely Cu-poor of Cu:In:Se = 23.4:26.5:50.1), which leads to a slightly peak shift.[17] However, the sample after the HASVS process (5%, 15%, 25% H_2) shows a nonsymmetry peak at In 3d owing to the formation of the indium oxide at a peak position of 444.7 eV, which is obtained from oxygen molecular dissociated by a Na catalyzed reaction. More Na accumulation near the CIGS surface will accelerate oxygenation of physisorbed O_2 molecules before the deposition of the buffer layer. In the case of CIGS, the thermodynamic driving force triggers the formation of the In−O bond. Consequently, the indium oxide was found on the surface of CIGS films. The formation of the indium oxide is enhanced with an increasing H_2 ratio and is finally balanced with the oxidation process because the effect of Na ions speeds up the oxidation process. Table 1 shows elemental concentrations extracted from XPS spectra for samples after the HASVS process with different H_2 ratios. Note that the Cu-poor surface is observed on the surface of the CIGS and the CGI ratio ([Cu]/([Cu]+[Ga]+[In])) slightly decreases as H_2 ratios increase from 0 to 15%, with which the bulk composition of the CIGS counterpart of ~0.9 was measured. In addition, Na concentration increases with increasing H_2 ratios and the Ga concentration decreases on the surface of the CIGS film after the HASVS process.

In addition, precisely quantitative depth profiles of CIGS thin films were measured by SIMS with the sputtering depth of ~700 nm as shown in Figures 3(a)-3(d), respectively. More

Table 1. XPS Surface Quantitative Elemental Results (Cu/In/Ga/Se/Na) of CIGS Films after the Conventional Selenization Process at a Pure N_2 Ambient and the Hydrogen-Assisted Selenization Process at Different H_2 Ratios

H_2 (%)	Cu (at%)	Ga (at%)	In (at%)	Se (at%)	Na	CGI[a]	GGI[b]
0	15.38	0.76	35.56	48.30	-	0.423	0.021
5	15.40	0.80	37.31	46.49	+	0.404	0.021
15	13.73	1.11	38.49	46.68	++	0.346	0.028
25	15.28	0.30	36.43	47.99	++	0.416	0.008

[a]CGI atomic ratio = Cu/(In+Ga). [b]GGI atomic ratio = Ga/(In+Ga).

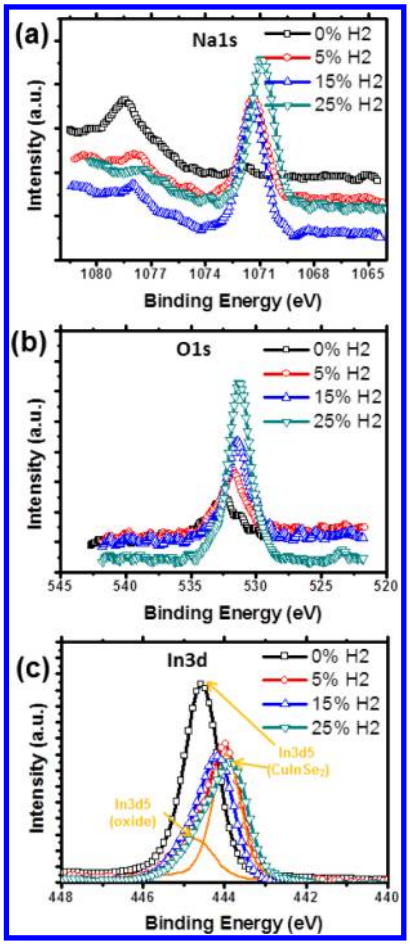

Figure 2. XPS spectra at (a) Na 1S, (b) O 1S, and (c) In 3d for CIGS films after the conventional selenization process at a pure N_2 ambient and the hydrogen-assisted selenization process in different H_2 concentrations.

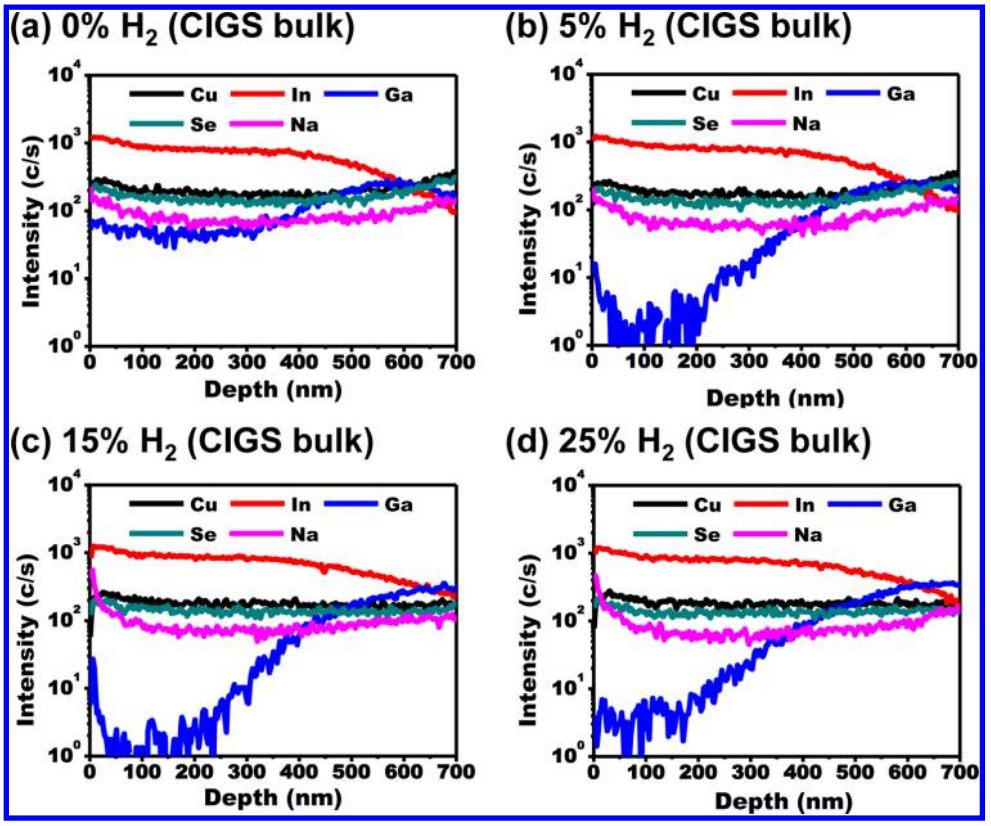

Figure 3. Bulk SIMS depth profiles of the CIGS surface for (a) pure N_2 ambient (0% H_2), (b) 5% H_2, (c) 15% H_2, and (d) 25% H_2, respectively.

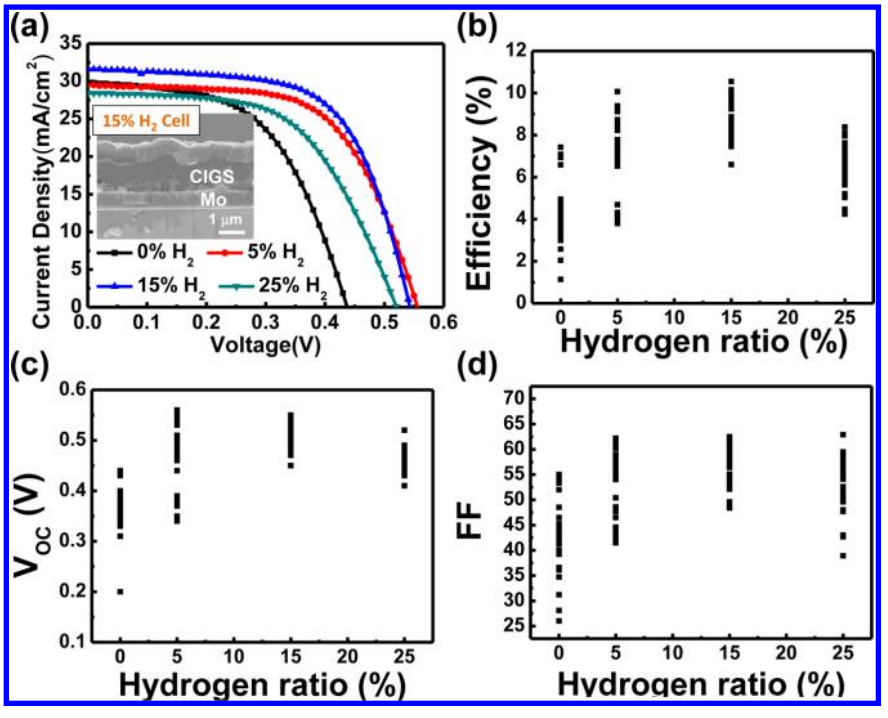

Figure 4. (a) Representative J-V characteristics of CIGS devices after the hydrogen-assisted selenization process at different H_2 concentrations. (b), (c), and (d) show statistic results at efficiencies, fill factors, and open circuit voltages for CIGS devices after the conventional selenization process in the pure N_2 ambient and the hydrogen-assisted selenization process in different H_2 concentrations.

uniform depth profiles of In and Se atoms were obtained from all samples except for depth profiles of Na, Cu, and Ga. By checking the near-surface depth profile, accumulation of Na concentrations and depletion of Cu concentrations with an increase of H_2 ratios near the surface of the CIGS was observed by SIMS, which is also consistent with XPS results (Figure S3). Oxygen molecules absorbed by the accumulation of Na atoms may also result in oxidation of In, namely formation of In−O bonding, owing to a electronegativity difference between In and O (1.7 for In and 3.5 for O). Thus, the formation of In−O

dx.doi.org/10.1021/am405780z | ACS Appl. Mater. Interfaces 2014, 6, 4842−4849

Table 2. Optimized Open Circuit Voltage (V_{oc}), Fill Factor (FF), and Dark Current Density (J_0) for CIGS Films after the Hydrogen-Assisted Selenization Process at Different H_2 Ratios

cond.	η (%)	FF	V_{oc} (mV)	J_{sc} (mA/cm^2)	R_{sh} (Ω/cm^2)	R_s (Ω/cm^2)	J_o (μA/cm^2)
0% H_2	7.1	53.9	440.0	29.8	260.0	1.6	44.0
5% H_2	10.1	61.0	560.0	29.5	307.5	2.2	0.1
15% H_2	10.8	63.3	540.0	31.6	400.0	0.8	7.1
25% H_2	8.4	56.7	520.0	28.4	777.6	3.2	14.1

bonding may alter bonding characteristics between In−Se and Cu−Se, which explains why Cu atoms diffuse out of their corner lattice sites of the chalcopyrite structure, resulting in copper poor on the surface of the CIGS.[15] Once the H_2 ratio reaches 25%, a decrease in Ga concentration on the surface of the CIGS film with increasing H_2 ratios can be found, and the Ga concentration at the surface of the CIGS becomes very low. Compared with the selenization process in a pure N_2 ambient, the Ga concentration profile still remains with uniform distribution through the whole film. The Ga atoms accumulated at the bottom of the CIGS film can be observed due to the preferential reaction between In and Se.[18] It might lead to phase segregation into $CuInSe_2$ (surface region) and $CuGaSe_2$ (back-contact region) in a severe case, which inhibits the realization of a high open circuit solar cell device.[19,20] In addition, no phase segregation in our case can be found according to the XRD result where only a single CIGS phase without the peak split due to phase segregation was found.

3.2. Efficiency Measurements of the CIGS Solar Cell after the Nontoxic Hydrogen-Assisted Solid Se Vapor Selenization Process. To shed light on how the HASVS process enhances energy conversion performance, HASVS processes at different H_2 ratios were applied at CIGS solar cells, followed by standard device fabrication processes, namely deposition of the CdS buffer layer, with a thicknesses of ~80 nm by the CBD method at 70 °C as the buffer layer and deposition of ZnO (70 nm)/ITO (550 nm) layers by pulsed-DC and DC sputtering systems as window/transparent conducting layers, respectively. The more than 50 devices with an actively measured area of 0.48 cm^2 uniformly selected from CIGS panels (30 cm × 40 cm) were measured (Figure S4). The representative I−V results are shown in Figure 4(a), and the optimized open circuit voltage (V_{oc}), short circuit current (J_{sc}), shunt resistance (R_{sh}), series resistance (R_s), dark current (J_0), filling factor (FF), and efficiency (η) at different conditions were tabulated in Table 2, respectively. The corresponding statistic results in η, FF, and V_{OC} are shown in Figure 4(b) to 4(d). Findings distinctly indicate that the efficiency can be enhanced after the HASVS process while the efficiency decreases as the HASVS process with a H_2 ratio >15%, which will be discussed later. As a result, the optimized efficiency from ~7.1% to ~10.8% (12.0% for active area) with over 30% enhancement at H_2 ratios of 5−15% can be measured. In addition, the increase of the shunt resistance (R_{sh}) due to the compact microstructure enhanced by hydrogen-assisted solid Se vapor diffusion (Figure 1) after the HASVS process is another reason to improve the efficiency with the enhanced fill factor.

At a high temperature crystallization process, the diffusion of gallium and indium is higher in sodium-free films than that in films containing sodium.[21] A downward diffusion of Ga from the surface of the CIGS film caused by high concentration of Na atoms and accumulated on the surface of the CIGS film after the HASVS process at a H_2 ratio of 25% leads to a low band gap, which limits the V_{oc}, resulting in lower efficiency. Furthermore, photolumiscence (PL) mapping was used to inspect how the uniformity of the whole device, with which PL intensities ratio at different positions directly reflect the quality of the device performance after the HASVS process at different H_2 ratios as shown in Figure 5. The corresponding PL spectra

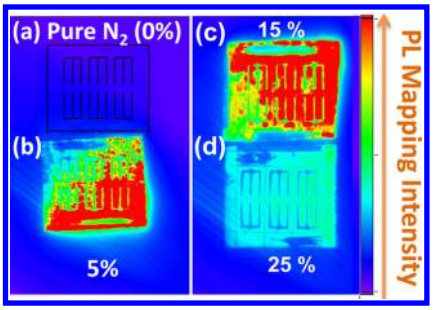

Figure 5. PL mapping for CIGS devices after the selenization processes (a) in the pure N_2 ambient and (b)−(d) the hydrogen-assisted selenization process in different H_2 concentrations.

are shown in Figure S5, for which the different spectra resulting from different emitting mechanisms are extracted. Obviously, the CIGS solar cell after the HASVS process with the 15% H_2 ratio shows the strongest intensity with the largest uniformity (Figure 4 b).

3.3. Widened Buried Homojunction Layer after the Nontoxic Hydrogen-Assisted Solid Se Vapor Selenization Process. It is supposed that the copper poor phenomenon (more copper vacancies) could form more Cd_{Cu} substitutions, leading to formation of buried homojunction followed by the CBD-CdS process, for which Cd ions can diffuse into the CIGS absorber layer owing to the similar ionic radii of Cd^{2+} (0.097 nm) and Cu^+ (0.096 nm) so that a thin n-type inversion layer can be formed. The n-type inversion layer was confirmed by XPS spectra at Cd 3d peaks[22,23] and can contribute a large number of free electrons to the surface due to different valence electrons between Cu and Cd ions, thus enhancing cell performance without detrimental recombination centers in the CdS/CIGS interfaces.[24−26]

Transmission electron microscopy (TEM) images are imperative to directly provide images of how the buried homojunction layer caused by internal diffusion of Cu and Cd atoms forms after the HASVS process. TEM images of the buried homojunction layer with different chemically elemental profiles for samples after the selenization in the pure N_2 ambient (0% H_2) and the HASVS process with 15% H_2 ratio were measured as shown in Figures 6(a) and 6(b), and the corresponding EDS elemental depth profiles are shown in Figures 6(c) and 6(d). The buried homojunction layer of ~20 nm for the CIGS film after the selenization process in a pure N_2 ambient (0% H_2) and the CdS layer can be observed by carefully scrutinizing the EDS elemental profile (Figure 6c), while the buried homojunction layer can be widened into ~60

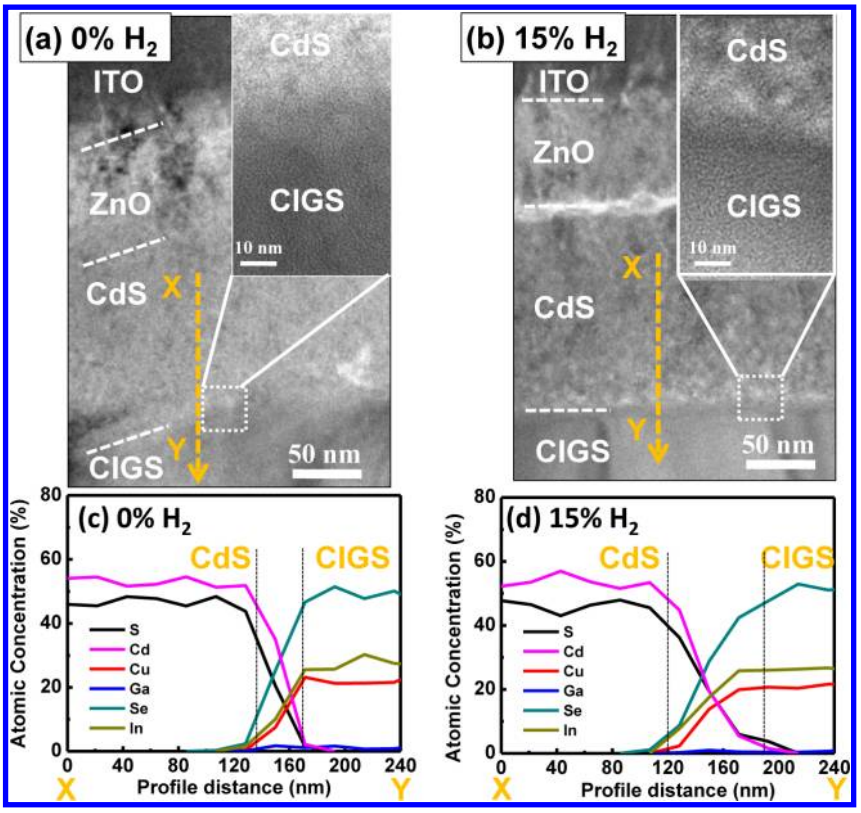

Figure 6. TEM images of top CIGS, CdS buffer layer, and TCO layers for CIGS films after (a) the selenization process in the pure N_2 ambient and (b) the hydrogen-assisted selenization process in the 15% H_2 ambient. (c) and (d) show the corresponding TEM/EDS compositional profiles films after the selenization process in the pure N_2 ambient and the hydrogen-assisted selenization process in the 15% H_2 ambient.

nm after the HASVS process (Figure 6d). The widened buried homojunction layer can be explained due to the formation of the Cu poor surface, which results in more Cd_{Cu} substitutions, triggering more Cd ions diffusing into the CIGS layer confirmed by XPS analysis (Figure S6). It is noteworthy that this buried homojunction depth could be further adjustable by varying the H_2/N_2 ratio, leading to different Cu-poor concentrations.

3.4. Junction Characteristics of CIGS Solar Cells after the Nontoxic Hydrogen-Assisted Solid Se Vapor Selenization Process. The remarkable improvement of the efficiency and filling factor comes from the improved V_{oc} and reduced J_0 owing to (1) the decrease of the interface recombination raised from the formation of the buried homojunction and (2) the enhanced separation of electron and hole carriers by the back surface field resulting from the accumulation of Na atoms on the surface of the CIGS film. The proof of the suppressed interface recombination and the better field profile in the space charge region for separation of electron−hole pairs are confirmed by carrier lifetime measurements from time-resolved photoluminescence (TRPL) as shown in Figure 7(a), for which the slow and fast components, $\tau 1$ and $\tau 2$, found to be 2.09/0.95 ns were measured for CIGS cells after the selenization in a pure N_2 ambient, while CIGS cells after 5%, 15%, and 25% H_2 HASVS processes were found to be 63.63/13.58 ns, 138.58/22.20 ns, and 8.78/2.53 ns as shown in the inset (Figure 7b), respectively.[27,28] Therefore, the decrease of interface/surface recombination velocity as the buried homojunction formation is expected to increase the minority carrier lifetime, resulting in an enhancement of open circuit voltage, $V_{OC,}$ to reduce the saturation current. On the

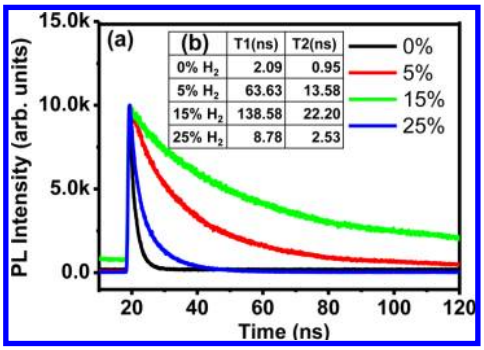

Figure 7. TRPL of carrier lifetime measurement for (a) without and (b) with hydrogen-assisted Se vapor selenization. A longer carrier lifetime is measured in the hydrogen assisted selenization sample.

other hand, the enhanced separation of electron and hole carriers resulting from the accumulation of Na atoms on the surface of the CIGS film can increase the free carrier density, which is further confirmed by drive level capacitance profiling (DLCP) measurements in a high frequency range (see Supporting Information, Figure S7).[15,29] As a result, the N_{DL} (drive level density) as high as $\sim 3.0 \times 10^{16}$ cm^{-3} can be measured in a hydrogen enhanced selenized (15% H_2) sample, which is three times larger than that of the CIGS devices after the conventional selenization processes in the pure N_2 ambient (0% H_2) with the drive level density of $\sim 1.0 \times 10^{16}$ cm^{-3}.

Finally, this methodology was also applied to CIS ($CuInSe_2$) thin film solar cells, for which enhanced efficiencies from 5.3% to 8.5% (9.4% for active area) with improved open circuit voltage, filling factor, and conversion efficiency of ~24%, ~34%, and ~60% can be achieved, respectively (see Supporting

Information, Figure S8). We believe that this work can provide a facile approach to improve the quality of CIGS and stimulate the nontoxic progress in the large scale CIGS PV industry.

4. CONCLUSIONS

We have demonstrated a nontoxic hydrogen-assisted Se vapor selenization process (HASVS) technique with solid Se pellets as the precursor at tunable H_2/N_2 ratios to achieve a large-area (40×30 cm^2) CIGS solar panel with improved open circuit voltage, filling factor, and conversion efficiencies of ~23%, ~17%, and ~50%, respectively, yielding enhanced efficiencies from 7.1% to 10.8% (12.0% for active area). An obvious diffusion of Na atoms from the substrate to the CIGS thin films was observed, leading to the widened Cu-poor region accompanied with the diffusion of Cd atoms from the CdS layer at the top surface of the CIGS thin film and forming an inversion layer, namely the buried homojunction. In addition, the Na concentration increases, while the Cu concentration decreases on the surface of the CIGS film after the HASVS process with increasing H_2 concentrations. As a result, a CGI ratio ([Cu]/([Cu]+[Ga]+[In]) of ~0.4 on the surface of the CIGS can be formed. Furthermore, the buried homojunction layer can be widened into ~60 nm after the HASVS process. The buried homojunction layer with a suitable width after the HASVS can be contributed to the formation of the Cu poor surface, which results in more Cd_{Cu} substitutions, triggering more Cd ions diffusing into the CIGS layer. The remarkable improvement of the efficiency and filling factor comes from the improved V_{oc} and reduced J_0 owing to (1) the decrease of the interface recombination raised from the formation of the buried homojunction and (2) the enhanced separation of electron and hole carriers by the back surface field resulting from the accumulation of Na atoms on the surface of the CIGS film. This one step HASVS process without additional hydrogen treatment can fulfill the demand of uniformity in larger scale with a lower cost process.

■ ASSOCIATED CONTENT

Ⓢ Supporting Information

EDS results; XRD spectra; CIGS solar cell panels; statistic results at J_{sc} for CIGS devices after the conventional selenization process; DLCP of carrier concentration measurement, low temperature PL; J-V measurements of $CuInSe_2$ solar cells after the hydrogen-assisted Se vapor selenization process. This material is available free of charge via the Internet at http://pubs.acs.org.

■ AUTHOR INFORMATION

Corresponding Authors

*E-mail: jmshieh@ndl.narl.org.tw.
*E-mail: chshen@ndl.narl.org.tw.
*E-mail: ylchueh@mx.nthu.edu.tw.

Notes

The authors declare no competing financial interest.

■ ACKNOWLEDGMENTS

The authors gratefully thank the National Science Council, Taiwan under Grants of NSC 101-2218-E-007-009-MY3, 102-2633-M-007-002, 101-2622-E-492-001-CC2 and National Tsing Hua University through Grant No. 102N2022E1. Y. L. Chueh greatly appreciates the use of the facility at CNMM the National Tsing Hua University through Grant No. 102N2744E1.

■ REFERENCES

(1) Akhavan, V. A.; Goodfellow, B. W.; Panthani, M. G.; Reid, D. K.; Hellebusch, D. J.; Adachibc, T.; Korgel, B. A. Spray-Deposited $CuInSe_2$ Nanocrystal Photovoltaics Energy. *Environ. Sci.* **2010**, *3*, 1600−1606.
(2) Beiley, Z. M.; McGehee, M. D. Modeling Low Cost Hybrid Tandem Photovoltaics with the Potential for Efficiencies Exceeding 20% Energy. *Environ. Sci.* **2012**, *5*, 9173−9179.
(3) Green, M. A.; Emery, K.; Hishikawa, Y.; Warta, W.; Dunlop, E. D. Solar Cell Efficiency Tables (Version 42). *Prog. Photovoltaics* **2013**, *21*, 827−837.
(4) Adurodija, F. O.; Carter, M. J.; Hill, R. A Novel Method of Synthesizing p-CuInSe2 Thin Films from the Stacked Elemental Layers Using a Closed Graphite Box. *1st IEEE Photovoltaic Spec. Conf.* **1994**, 186−189.
(5) Chichibu, S. F.; Sugiyama, M.; Ohbasami, M.; Hayakawa, A.; Mizutani, T.; Nakanishi, H.; Negami, T.; Wada, T. Use of Diethylselenide as a Less-Hazardous Source for Preparation of $CuInSe_2$ Photo-Absorbers by Selenization of Metal Precursors. *J. Cryst. Growth* **2002**, *243*, 404−409.
(6) Birkmire, R. W.; Eser, E. Polycrystalline Thin Film Solar Cells: Present Status and Future Potential. *Annu. Rev. Mater. Sci.* **1997**, *27*, 625−653.
(7) Huang, C. H.; Shih, Y. C.; Chuang, W. J.; Lin, C. P. Impacts of Process Parameters on CIGS Solar Cells Prepared by Selenization Process with Se Vapor. *10th Proc. - Int. Conf. Solid-State Integr. Circuit Technol.* **2010**, 2019−2021.
(8) Nakamura, N.; Takahama, T.; Isomura, M.; Nishikuni, M.; Yoshida, K.; Tsuda, S.; Nakano, S.; Ohnishi, M.; Kuwano, Y. The Influence of the Si-H Bond on the Light-Induced Effect in a-Si Films and a-Si Solar Cells. *Jpn. J. Appl. Phys.* **1989**, *28*, 1762−1768.
(9) Otte, K.; Lippold, G.; Newmann, H.; Schindler, A. Hydrogen in $CuInSe_2$. *J. Phys. Chem. Solids* **2003**, *64*, 1641−1647.
(10) Kilic, C.; Zunger, A. N-Type Doping and Passivation of $CuInSe_2$ and $CuGaSe_2$ by Hydrogen. *Phys. Rev. B* **2003**, *68*, 075201.
(11) Lee, D. W.; Seol, M. S.; Kwak, D. W.; Oh, J. S.; Jeong, J. H.; Cho, H. Y. Hydrogen Effects on Deep Level Defects in Proton Implanted $Cu(In,Ga)Se_2$ Based Thin Films. *Thin Solid Films* **2012**, *520*, 6382−6385.
(12) Bob, B.; Lei, B.; Chung, C. H.; Yang, W.; Hsu, W. C.; Duan, H. S.; Hou, W. W. J.; Li, S. H.; Yang, Y. The Development of Hydrazine-Processed $Cu(In,Ga)(Se,S)_2$ Solar Cells. *Adv. Energy Mater.* **2012**, *2*, 504−522.
(13) Yoon, J. H.; Cho, S.; Seong, T. Y.; Jeong, J. H. *Optical Diagnosis of the Microstructure of Mo Back Contact for CIS Solar Cell 216th ECS Meeting*, 2009.
(14) Baji, Z.; Lábadi, Z.; Molnár, G.; Pécz, B.; Tóth, A. L.; Tóth, J.; Csik, A.; Bársony, I. Post-Selenization of Stacked Precursor Layers for CIGS. *Vacuum* **2013**, *92*, 44−51.
(15) Kronik, L.; Cahen, D.; Shock, H. W. Effects of Sodium on Polycrystalline $Cu(In,Ga)Se_2$ and Its Solar Cell Performance. *Adv. Mater.* **1998**, *10*, 31−36.
(16) Osenbach, J. W.; Voris, S. S. Sodium Diffusion in Plasma-Deposited Amorphous Oxygen-Doped Silicon Nitride (a-SiON:H) Films. *J. Appl. Phys.* **1988**, *63*, 4494−4500.
(17) Kohiki, S.; Nishitani, M.; Negami, T.; Wada, T. X-ray Photoelectron Spectroscopy of $CuInSe_2$. *Phys. Rev. B* **1992**, *45*, 9163−9168.
(18) Hanket, G. W.; Shafarman, W. N.; McCandless, B. E.; Birkmire, R. W. Incongruent Reaction of Cu-(InGa) Intermetallic Precursors in H_2Se and H_2S. *J. Appl. Phys.* **2007**, *102*, 074922.
(19) Kim, W. K.; Hanket, G. M.; Shafarman, W. N. Ga Homogenization by Simultaneous H_2Se/H_2S Reaction of Cu-Ga−In Precursor Sol. *Energy Mater. Sol. Cells* **2011**, *95*, 235−238.

(20) Marudachalam, M.; Birkmire, R. W.; Hichri, H.; Schultz, J. M.; Swartzlander, A.; Al-Jassim, M. M. Phases, Morphology, and Diffusion in $CuIn_xGa_{1-x}Se_2$ Thin Films. *J. Appl. Phys.* **1997**, *82*, 2896−2905.
(21) Lundberg, O.; Lu, J.; Rockett, A.; Edoff, M.; Stolt, L. Diffusion of Indium and Gallium in CIGS Thin Film Solar Cells. *J. Phys. Chem. Solids* **2003**, *64*, 1499−1504.
(22) Lee, D. Y.; Kim, M. S.; Larina, L.; Ahn, B. T. Effects of Cu Content on the Photovoltaic Properties of $Cu(In,Ga)Se_2$ Solar Cells Prepared by the Evaporation of Binary Selenide Sources Electron. *Mater. Lett.* **2008**, *4*, 13−18.
(23) Sozzi, G.; Troni, F.; Menozzi, R. Numerical Analysis of the Effect of Grain Size and Defects on the Performance of CIGS Solar Cells Proc. *CS-MANTECH Conf.* **2010**, 353−356.
(24) Schmid, D.; Ruckh, M.; Grunwald, F.; Schock, H. W. Chalcopyrite/Defect Chalcopyrite Heterojunction on the Basis of $CuInSe_2$. *J. Appl. Phys.* **1993**, *73*, 2902−2909.
(25) Yan, Y.; Jones, K. M.; Abushama, J.; Young, M.; Asher, S.; Al-Jassim, M. M.; Noufi, R. Microstructure of Surface Layers in $Cu(In,Ga)Se_2$ Thin Films. *Appl. Phys. Lett.* **2002**, *81*, 1008−1010.
(26) Liao, D.; Rockett, A. Cu Depletion at the $CuInSe_2$ Surface. *Appl. Phys. Lett.* **2003**, *82*, 2829−2831.
(27) Ohnesorge, B.; Weigand, R.; Bacher, G.; Forchel, A.; Riedl, W.; Karg, F. H. Minority-Carrier Lifetime and Efficiency of $Cu(In,Ga)Se_2$ Solar Cells. *Appl. Phys. Lett.* **1998**, *73*, 1224−1226.
(28) Shirakataa, S.; Nakada, T. Time-Resolved Photoluminescence in $Cu(In,Ga)Se_2$ Thin Films and Solar Cells. *Thin Solid Films* **2007**, *515*, 6151−6154.
(29) Jiang, C.-S.; Noufi, R.; AbuShama, J. A.; Ramanathan, K.; Moutinho, H. R.; Pankow, J.; Al-Jassim, M. M. Local Built-in Potential pn Grain Boundary of $Cu(In,Ga)Se_2$ Thin Films. *Appl. Phys. Lett.* **2004**, *84*, 3477−3479.